Stress-Induced Anisotropy of Electromigration in Copper Interconnects

H. Ceric, R. Lacerda de Orio, J. Cervenka, and S. Selberherr

Institute for Microelectronics, TU Wien, Gußhausstraße 27–29/E360
A-1040 Wien, Austria
Fax: +43-1-58801/36099,Phone: +43-1-58801/36032
Email: Ceric@iue.tuwien.ac.at

Abstract. Modern interconnect structures are exposed to high mechanical stresses during their operation. These stresses have their sources in interconnect process technology and electromigration. The mechanical properties of passivating films and the choice of process technology influence electromigration reliability. In this paper we analyze the interplay between electromigration and mechanical stress on the atomic level. A stress-dependent diffusion tensor has been derived and implemented in a continuum electromigration model. Since the vacancy dynamics at grain boundaries also contributes to the stress distribution, the electromigration model has been extended by a grain boundary model. The plausibility of the compound model is demonstrated with a simulation example of stress dependent electromigration in a three-dimensional, dual-damascene interconnect structure.

Keywords: simulation, electromigration, stressmigration
PACS: 66.30.Qa

INTRODUCTION

There are three major sources of mechanical stress in passivated interconnect lines. The first one is the thermal stress, resulting from the difference in thermal expansion between the passivation and the metal upon cooling from high deposition temperatures. Metalization processing can expose an integrated circuit to temperatures of more than 500 °C. The second source of stress is nonequilibrium film growth. As wafer curvature measurements have shown this source of stress is even more important than the thermal stress. The third major source of stress is electromigration itself.

Although the measurements significantly contribute to the understanding of thin film stresses, they are, in most cases, limited to simple test structures. Furthermore, the detailed stress distribution within a material cannot be experimentally determined.

The evolution of mechanical stress in interconnect lines depends on whether or not vacancies can be created or annihilated such that their equilibrium is maintained. For mechanical stresses to develop, there must be both a volume expansion or contraction of the line with respect to the surrounding material and a mechanical constraint applied by the surrounding material. As atoms exchange place with vacancies and move towards the anode end of the line, there is a flow of vacancies towards the cathode end. In the absence of vacancy sources and sinks, this would result in a vacancy supersaturation on the cathode end and a deficiency at the anode end. Since the replacement of an atom with a vacant site produces a small relaxation in the surrounding lattice, there would be a net volume contraction at the cathode and expansion at the anode.

For the dual damascene technology high tensile stresses at the interfaces, where one can expect defects, are generally critical. Electromigration and stressmigration can increase this local tensile stress or act against each other in order to reduce tensile stress.

The choice of passivating film material and corresponding process technology causes tensile or compressive stress in the interface between the passivating film and the interconnect metal. Interfacial compressive stress diminishes electromigration along interfaces by reducing the diffusivity [1]. However, numerous experimental observations have shown [2] that tensile stress in the interface increases the possibility of failure. Increased thickness and rigidity of the capping layer prevent relaxation of both thermal and electromigration induced stress, which results in dielectric cracking and metal extrusion.

The fact that an anisotropically stressed solid causes anisotropy of diffusional material transport has been confirmed

CP1143, *Stress-Induced Phenomena in Metallization: 10th International Workshop,* edited by P. S. Ho, S. Ogawa, and E. Zschech
© 2009 American Institute of Physics 978-0-7354-0680-3/09/$25.00

with experimental and theoretical studies. In early attempts only models with a dependence caused by the spherical-part of the stress tensor on diffusivity were used. Later studies which have considered the detailed atomic configuration of the stressed crystal lattice have shown the dependence of the diffusivity on the stress tensor. Both stressmigration and electromigration are affected by this diffusional anisotropy.

The mechanical stresses generally change the local atomic configuration and this makes copper interfaces to surrounding layers with their complex transitional structures prone to the influence of anisotropic stress. Grain boundaries represent high diffusivity paths and potential sites of vacancy production. The chances of grain boundaries to trap, transport, and release vacancies also depend on the local stress configuration.

In this paper we introduce and discuss an electromigration model in which the anisotropy of material transport is induced by the anisotropy of the local stress field. The model is derived based on considerations on the atomic level.

STRAIN INDUCED ANISOTROPY OF ELECTROMIGATION

A careful analysis of vacancy diffusion [3] based on classical thermodynamics provides the following expression

$$D_v = \gamma a^2 \Gamma \exp\left(-\frac{\Delta G}{kT}\right) \quad (1)$$

where γ is a geometrical constant of order unity, a is the lattice parameter, and Γ is the vibrational frequency. $\Delta G = \Delta G_f + \Delta G_m$, where ΔG_f and ΔG_m are increments of Gibbs free energy of vacancy formation and vacancy migration. The diffusion of vacancies is studied as an isobaric and isothermal process [4] and, therefore, the starting point of the analysis is the Gibbs free energy,

$$G = F + pV, \quad (2)$$

which is determined by the free energy F, the pressure p, and the volume V. The vacancy formation causes the volume change V_f, and vacancy migration the volume change V_m. For the vacancy diffusivity under the influence of an external pressure p we obtain from (1) and (2)

$$D_v = \gamma a^2 \Gamma \exp\left(-\frac{\Delta F + p(V_f + V_m)}{kT}\right), \quad (3)$$

with $\Delta F = \Delta F_f + \Delta F_m$, where ΔF_f and ΔF_m are changes of the free energy upon vacancy formation and vacancy migration, resepectively.

Instead of a scalar point defect (vacancy) formation volume, Aziz [5, 6] introduced a formation strain tensor $\bar{\bar{V}}_f$

$$\bar{\bar{V}}_f = \pm\Omega \begin{bmatrix} 0 & & \\ & 0 & \\ & & 1 \end{bmatrix} + \frac{V^r}{3} \begin{bmatrix} 1 & & \\ & 1 & \\ & & 1 \end{bmatrix}. \quad (4)$$

The sign + is for vacancy formation and the sign - is for interstitial formation. V^r is the relaxation volume which propagates elastically to all surfaces and provides equal contributions along all axes, on average, after point defect equilibration.

Similarly to the formation strain tensor, Aziz [5, 6] also introduced the migration strain tensor $\bar{\bar{V}}_m$

$$\bar{\bar{V}}_m = \begin{bmatrix} V_\perp^m & & \\ & V_\perp^m & \\ & & V_\parallel^m \end{bmatrix}, \quad (5)$$

where $V_\perp^m$ and $V_\parallel^m$ are the volume changes perpendicular and parallel to the diffusion direction, respectively. The dependence of the vacancy diffusivity D_v on hydrostatic preassure (3) can also be extended for a general stress field $\bar{\bar{\sigma}}$.

$$D_v = \gamma a^2 \Gamma \exp\left(-\frac{\Delta F + \bar{\bar{\sigma}} : (\bar{\bar{V}}_f + \bar{\bar{V}}_m)}{kT}\right) \quad (6)$$

The relationship (3) is used in numerous electromigration models [7, 8, 9, 10], however it only describes the influence of scalar hydrostatic pressure on the scalar diffusivity.

As the analysis on the atomic level carried out by Schroeder and Dettman [11] has revealed, the vacancy flux $\vec{J}_v$ is separated in a diffusive part and a drift part

$$J_{v,i} = J_{v,i}^{\mathrm{diff}} + J_{v,i}^{\mathrm{drift}} = -\sum_j D_{ij}^v \frac{\partial C_v}{\partial x_j} - \frac{C_v}{kT} \sum_j D_{ij}^v \frac{\partial E_e}{\partial x_j}. \tag{7}$$

Instead of a scalar diffusivity (6), here we have a diffusivity tensor $\bar{\bar{D}}^v$ with the components

$$D_{ij}^v = \frac{6D_0^v}{Z} \sum_{k=1}^{Z} a_i^k a_j^k \exp\Big(-\frac{E_s^k - E_e}{kT}\Big). \tag{8}$$

a_i^k are the normalized components of the jump vector $\vec{r}_k$ (Fig. 1), and Z is the number of neighbouring sites. D_0^v is the vacancy diffusivity in the ideal crystal lattice [4]

$$D_0^v = \frac{1}{12} Z \Gamma \lambda^2, \tag{9}$$

where λ is the vacancy jump length.

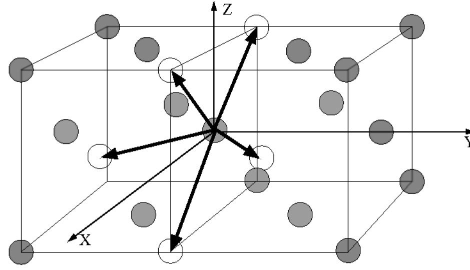

FIGURE 1. Jump vectors in face-centered cubic (fcc) crystals.

The application of a stress field $\bar{\bar{\sigma}}$ generally causes a distorsion of the saddle point energy E_s^k and the valley point energy E_e [11]. As one can see from (7), stress as a driving force acts only on the valley point energy E_e.

When a defect is created, the solid changes shape from its original condition (Fig. 2). In linear elasticity theory, the change in the shape of a volume can be expressed with a real, symmetric tensor. For example, the distorsion of a sphere into an ellipsoid produces a new volume $\bar{\bar{\Omega}}$ [13]

$$\bar{\bar{\Omega}} = \begin{bmatrix} \Omega_1 & & \\ & \Omega_2 & \\ & & \Omega_3 \end{bmatrix}. \tag{10}$$

Generally the symmetry of the shape change due to defect production depends on the symmetry of the defect.

The change of energy at the saddle point and the valley point is determined as an addtitional energy needed to create the defect in the presence of an external stress $\bar{\bar{\sigma}}$,

$$E_s^k(\bar{\bar{\sigma}}) = E_s(0) + \bar{\bar{\Omega}}_s^k : \bar{\bar{\sigma}}, \tag{11}$$

$$E_e(\bar{\bar{\sigma}}) = E_e(0) + \bar{\bar{\Omega}}_e : \bar{\bar{\sigma}}, \tag{12}$$

where the stress is evaluated locally. $E_s^k(0)$ and $E_e(0)$ are the creation energies in the absence of external stresses. $\bar{\bar{\Omega}}_s^k$ and $\bar{\bar{\Omega}}_e$ are the changes in volume/shape imposed on the perfect, stressed crystal by placing the defect at the saddle point and the valley point, respectively. They are not equal to the creation and migration volumes [13].

The applied stress changes the energies at the saddle site and the valley site. The volume change caused by placing a vacancy at a valley site can be expressed as $\bar{\bar{\Omega}}_e = \Omega \bar{\bar{\varepsilon}}_e^I$, where $\bar{\bar{\varepsilon}}_e^I$ is the induced strain. In order to fully consider the

influence of anisotropic stress on saddle site energies, the strain induced by placing a vacancy on the saddle point must depend on the jump direction $\vec{a}_k$, e.g. $\Omega \bar{\bar{\varepsilon}}_s^I \cdot \vec{a}_k$, (Fig. 2). $\bar{\bar{\varepsilon}}_s^I$ and $\bar{\bar{\varepsilon}}_e^I$ are determined as

$$\bar{\bar{\varepsilon}}_s^I = \begin{bmatrix} \varepsilon_s & & \\ & \varepsilon_s & \\ & & \varepsilon_s \end{bmatrix}, \quad \bar{\bar{\varepsilon}}_e^I = \begin{bmatrix} \varepsilon_e & & \\ & \varepsilon_e & \\ & & \varepsilon_e \end{bmatrix}, \tag{13}$$

since the vacancy exibits at the valley as well as at the saddle site a cubic symmetry. Now (12) and (11) can be rewritten as

$$E_s^k(\bar{\bar{\sigma}}) = E_s(0) + \Omega(\bar{\bar{\varepsilon}}_s^I \cdot \vec{a}_k) \cdot (\bar{\bar{\sigma}} \cdot \vec{a}_k). \tag{14}$$

$$E_e(\bar{\bar{\sigma}}) = E_e(0) + \Omega \mathrm{tr}(\bar{\bar{\sigma}}) \varepsilon_e, \tag{15}$$

By inserting these expressions into (8) one obtains

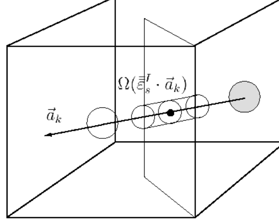

FIGURE 2. Volume change caused by placing a vacancy at the saddle point in a stressed fcc crystal.

$$D_{ij}^v = \frac{6D_0}{Z} \exp\left(-\frac{E_s(0) - E_e(0)}{kT}\right) \exp\left(\frac{\Omega \mathrm{tr}(\bar{\bar{\sigma}}) \varepsilon_e}{kT}\right) \sum_{k=1}^{Z} a_i^k a_j^k \exp\left(-\frac{\Omega(\bar{\bar{\varepsilon}}_s^I \cdot \vec{a}_k) \cdot (\bar{\bar{\sigma}} \cdot \vec{a}_k)}{kT}\right). \tag{16}$$

Further, equation (14) is set into (7)

$$J_{v,i} = -\sum_j D_{ij}^v \frac{\partial C_v}{\partial x_j} - \frac{C_v \Omega \varepsilon_e}{kT} \sum_j D_{ij}^v \frac{\partial \mathrm{tr}(\bar{\bar{\sigma}})}{\partial x_j}. \tag{17}$$

The complete flux driven by stressmigration and electromigration written in vector form is now

$$\vec{J}_v = -\bar{\bar{D}}^v \left(\nabla C_v + \frac{C_v \Omega \varepsilon_e}{kT} \nabla \mathrm{tr}(\bar{\bar{\sigma}}) + |Z^*| e \nabla \varphi\right), \tag{18}$$

where φ is the electric potential which obeys Laplace's equation ($\Delta\varphi = 0$) and Z^* is the effective vacancy charge.

Grain boundaries, as fast diffusion paths, play an important role in vacancy transport. They are capable of absorbing and emitting vacancies and thus they are also sites where stress build up takes place. For an accurate description of the stress distribution inside an interconnect the physics of grain boundaries must also be taken into account.

In [14] a new model is introduced where a grain boundary is treated as a separate medium with the capability of absorbing and releasing vacancies. We denote the vacancy concentration from both sides of the grain boundary as $C_{v,1}$ and $C_{v,2}$, respectively, and the concentration of immobile vacancies which are trapped inside the grain boundary as C_v^{im} (Fig. 3).

The dynamics of mobile vacancies (C_v) and immobile vacancies (C_v^{im}) in the presence of the grain boundary is given by the following equation,

$$\frac{\partial C_{v,\alpha}}{\partial t} = -\nabla \cdot \vec{J}_{v,\alpha} + \frac{1}{\tau}\left(C_v^{eq} - C_v^{im}\left(1 + \frac{2\,\omega_R}{\omega_T(C_{v,1} + C_{v,2})}\right)\right). \tag{19}$$

$\alpha = 1$ and $\alpha = 2$ indicate the left and the right side of the grain boundary, respectively, and τ is the relaxation time given by

$$\frac{1}{\tau} = \frac{\omega_T(C_{v,1} + C_{v,2})}{\delta}. \tag{20}$$

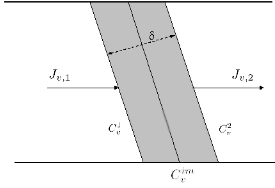

FIGURE 3. Grain boundary area.

Mobile vacancies are trapped from both neighboring grains with the trapping rate ω_T and released to these grains with a release rate ω_R. The capacity of the grain boundary to accept trapped vacancies is expressed by the stress-dependent equilibrium concentration

$$C_v^{eq} = C_v^0 \exp\Big(\frac{\sigma_{nn}\Omega}{k_B T}\Big), \quad \sigma_{nn} = \vec{n} \cdot \bar{\bar{\sigma}} \cdot \vec{n}, \tag{21}$$

where we assume a unique equilibrium vacancy concentration C_v^0 in stress free copper, both, in grain bulks and boundaries. $\vec{n}$ is the normal vector to the grain surface. The strain growth from both sides of the grain boundary is propotional to the growth rate of immobile vacancies,

$$\frac{\partial \varepsilon_{ij,\alpha}^v}{\partial t} = \frac{1}{3}\Omega\Big((1-f)\nabla \cdot \vec{J}_{v,\alpha} + f\frac{\partial C_v^{im}}{\partial t}\Big)\delta_{ij}. \tag{22}$$

The equations (19) and (22) are solved until a stress threshold for void nucleation is reached at some weak adhesion point at the copper/capping layer interface.

SIMULATION RESULTS AND DISCUSSION

The impact of thermo-mechanical stress on electromigration induced vacancy transport is illustrated with a typical dual-damascene interconnect structure (Fig. 4). Generally, each portion of interconnect is embedded in a surrounding which has spatially varying mechanical properties. This is caused by the three-dimensional character of interconnect layouts as well as different mechanical properties of materials used for dielectric, barrier, and capping layer. We have used the following parameters:

- Cu (interconnect) : Z^*=4, f=0.4, Ω=1.182x10^{-23}cm^3, E=125 GPa, ν=0.34;
- Ta (barrier): E=380 GPa, ν=0.27;
- Si_3N_4 (capping): E=380 GPa, ν=0.27;

The mechanical complexity of the interconnects surrounding is modeled by setting appropriate mechanical boundary conditions (Fig. 4). The layout under consideration is bounded by a rectangular box (800 nm x 100 nm x 400 nm), the top and the bottom of the box are mechanically fixed (Fig. 4). Before starting an actual electromigration simulation a thermo-mechanical simulation is carried out. The layout is cooled down from 120 ^{o}C to 20 ^{o}C. Due to mismatch of the thermal expansion coefficients of the different materials a mechanical stress is built up. In Fig. 5, Fig. 6, and Fig. 7, the σ_{xx}, σ_{yy}, and σ_{zz} components of the thermal stress tensor are shown, respectively. As we can see, the stress is anisotropic and tensile. Due to the geometry and boundary conditions the area of high tensile stress (over 400 MPa in Fig. 5) is spread throughout the via.

Stress influences electromigration in two ways it is an additional driving force and its presence is a source of anisotropy in diffusion. The importance of stress as a driving force was early recognized [15, 16, 17] and since then regularly included in electromigration models [18, 19]. However, from the atomic point of view, the effect of stress as a driving force can not be separated from the effect of crystal lattice distortion due to stress [12].

In order to demonstrate the influence of stress, we compare the vacancy distribution modeled with a simple pressure-dependent scalar diffusivity (Fig. 8a) with one obtained considering stress dependent tensorial diffusivity (Fig. 8b). In

both cases we have simulated upstream electromigration with an applied current density of 8 MA/cm^2. It can clearly be seen in Fig. 8 that the anisotropic diffusivity causes a significantly more widespread area of high vacancy concentration (threshold of $5e16$ cm^{-3}) than in the case of scalar diffusivity. Wider ares of atom depletion are more probable to match weak adhesion spots at capping/interconnect interfaces and induce void nucleation.

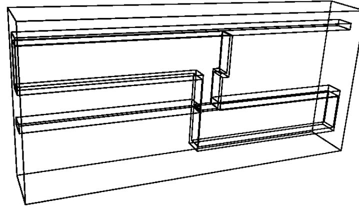

FIGURE 4. Dual-damascene layout used. Top and bottom of the structure are mechanically fixed for thermomechanical simulation.

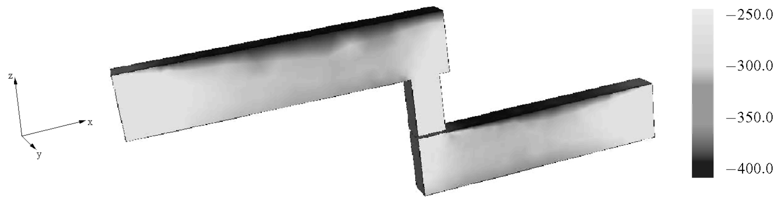

FIGURE 5. σ_{xx} component of thermomechanical stress tensor [MPa].

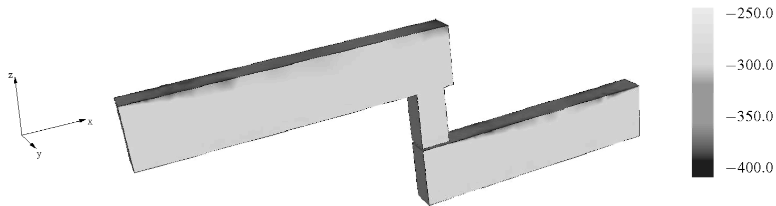

FIGURE 6. σ_{yy} component of thermomechanical stress tensor [MPa].

CONCLUSION

A careful analysis of the connection between the local vacancy dynamics and stress build-up has been carried out. The obtained relations have been coupled to an electromigration model using the concepts of stress driven diffusion and anisotropy of the diffusivity tensor. The model presented in this paper is also based on a detailed analysis of the vacancy dynamics at the grain boundaries and the related mechanisms of stress build-up at triple points. A dual-damascene architecture layout is used to illustrate and verify the introduced modeling approach.

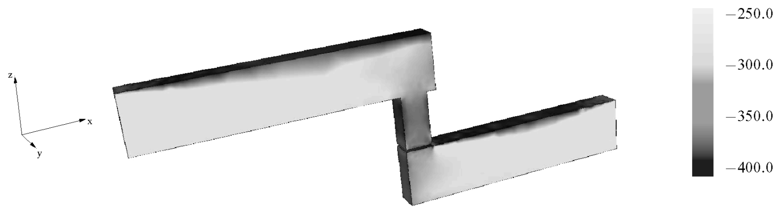

FIGURE 7. σ_{zz} component of thermomechanical stress tensor [MPa].

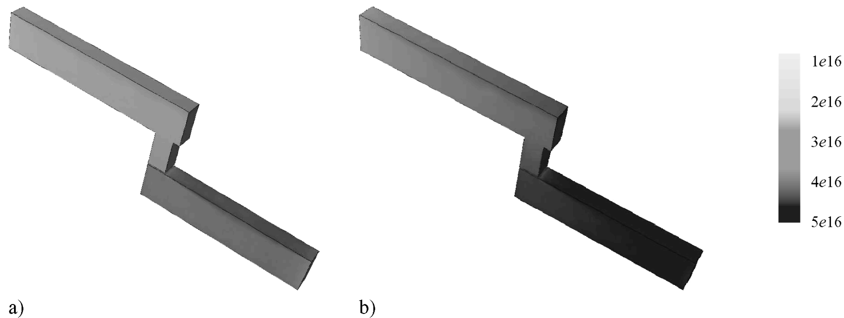

a) b)

FIGURE 8. Vacancy distribution after 10 min for the case of isotropic scalar diffusivity (a) and anisotropic tensorial diffusivity (b) [cm^{-3}]

REFERENCES

1. J. Lloyd and K. P. Rodbell, *in Handbook of Semiconductor Interconnection Technoogy, edited by G.C. Schwartz and K. V. Srikrishnan*, pp. 471–520, (2006).
2. J. Lloyd and J.J.Clement, *Thin Solid Films*, vol. **262**, pp. 135–141, (1995).
3. C. P. Flynn, *Point Defects and Diffusion*, Clarendon Press, Oxford, 1972, ISBN 0-198-51260-0.
4. M. E. Glicksman, *Diffusion in Solids*, John Wiley and Sons, Inc., 2000, ISBN 0-471-23972-0.
5. M. J. Aziz, *Appl. Phys. Lett.*, vol. **70**, pp. 2810–2812, (1997).
6. M. J. Aziz, *Proceedings SISPAD Conference*, pp. 137–142, (2003).
7. A. Kteyan, V. Sukharev, M. A. Meyer, E. Zschech, and W. D. Nix, *Stress-Induced Phenomena in Metallization, AIP*, pp. 42–55, (2007).
8. B. M. Clemens, W. D. Nix, and R. J. Gleixner, *Journal of Materials Research*, vol. **12**, pp. 2038–2042, (1997).
9. V. Petrescu and W. Schoenmaker, *Predictive Simulation of Semiconductor Processsing: Status and Challenges, Springer Series in Materials Sciences*, vol. **72**, pp. 387–456, (2004).
10. V. Sukharev, R. Choudhury, and C. W. Park, *Integrated Reliability Workshop Final Report, 2003 IEEE International*, pp. 80–85, (2003).
11. K. Schroeder and K. Dettmann, *Z. Physik B*, vol. **22**, pp. 343–350, (1975).
12. P. H. Dederichs and K. Schroeder, *Phys. Rev. B*, vol. **17**, pp. 2524–2536, (1978).
13. M. S. Daw, W. Windl, N. N. Carlson, M. Laudon, and M. P. Masquelier, *Phys. Rev. B*, vol. **64**, pp. 045205, (2001).
14. H. Ceric, R. L. de Orio, J. Cervenka, and S. Selberherr, *IEEE Trans. Mat. Dev. Rel.*, (2009).
15. I. A. Blech and C. Herring, *J. Appl. Phys.*, vol. **29**, pp. 131–133, (1976).
16. I. A. Blech, *J. Appl. Phys.*, vol. **47**, pp. 1203–1208, (1976).
17. I. A. Blech and K. L. Tai, *Appl. Phys. Lett.*, vol. **30**, pp. 387–389, (1976).
18. M. E. Sarychev and Y. V. Zhitnikov, *J. Appl. Phys.*, vol. **86**, pp. 3068–3075, (1999).
19. H. Ye, C. Basaran, and D. Hopkins, *IEEE Trans. on Comp. and Pack.*, vol. **26**, pp. 673 –681, (2003).